

Constraints on invisible $B^+ \rightarrow K^+ X$ decays from the Belle II $B^+ \rightarrow K^+ \nu \bar{\nu}$ measurement

Lorenz Gärtner  ^{1,*} Nikolai Krug  ^{1,†} Thomas Kuhr  ^{1,‡} Michael A. Schmidt  ^{2,§} Slavomira Stefkova  ^{3,¶} and Bruce Yabsley  ^{4,**}

¹*Ludwig Maximilians University, 80539 Munich, Germany*

²*University of New South Wales, Sydney, Australia*

³*University of Bonn, 53115 Bonn, Germany*

⁴*University of Sydney, Sydney, Australia*

Belle II measurement of the branching fraction for $B^+ \rightarrow K^+ \nu \bar{\nu}$ shows a 2.7σ excess over the Standard Model prediction and motivates new-physics explanations such as axion-like particles, Higgs-like scalars, or beyond Standard Model gauge bosons. A two-body decay $B^+ \rightarrow K^+ X$ with an invisible X provides a natural candidate explanation. This work provides a comprehensive test of this hypothesis using Belle II's public model-agnostic likelihood. Posterior distributions are derived for the resonance mass m_X and the branching fraction, and a modified frequentist upper-limit mass scan is performed. The data favor a resonance with mass $m_X = 2.1^{+0.2}_{-0.1}$ GeV and the product $\mathcal{B}(B^+ \rightarrow K^+ X) \cdot \mathcal{P}_{X,\text{inv}} = 9.2^{+1.8}_{-3.4} \cdot 10^{-6}$, where $\mathcal{P}_{X,\text{inv}}$ is the probability that X (and its decay products) are undetected. Bayes factors indicate a very strong preference for the Standard Model plus resonance over the Standard Model-only hypothesis. A frequentist likelihood-ratio test favors the Standard Model plus resonance hypothesis by 3.0σ . A light invisible resonance plus the Standard Model therefore provides a compelling description of the Belle II data.

I. INTRODUCTION

Flavor-changing neutral current processes are sensitive probes of physics beyond the Standard Model (SM) because they are suppressed in the SM. Rare meson decays with missing energy are particularly interesting because they are sensitive to new light particles that escape detection. One such process is $B^+ \rightarrow K^+ \nu \bar{\nu}$, for which the Belle II collaboration has reported evidence [1] for a 2.7σ excess over the SM.

A two-body decay $B^+ \rightarrow K^+ X$ [2, 3], involving a new light boson X , provides an attractive explanation for this observed excess. This scenario is defined by the boson mass m_X and the bsX interaction strength. While previous studies explored this model [2–7], they assumed a negligible width ($\Gamma_X \ll m_X$) and relied on approximations, as detailed experimental information was unavailable.

This work provides the first rigorous test of this hypothesis by exploiting the model-agnostic likelihood of the $B^+ \rightarrow K^+ \nu \bar{\nu}$ measurement published by the Belle II collaboration [8, 9]. This allows a quantification of the preferred parameter space for an invisible resonant contribution, described by a Breit-Wigner distribution with mass m_X and decay width Γ_X .

In Section II the theoretical background is presented. Section III describes the Belle II analysis, the reinterpretation method, and the resonance model. Bayesian credible intervals are derived in Section IV, and modified

frequentist upper limits from a mass scan are derived in Section V. Finally, goodness-of-fit and model comparison are assessed in Sections VI and VII, respectively, before concluding in Section VIII.

II. THEORETICAL BACKGROUND

Models explaining the excess with a two-body decay can be distinguished by the spin of the boson X , its decay width Γ_X , and the bsX coupling. Among spin-0 bosons, axion-like particles provide a well-motivated explanation for the excess [2, 10–13]. The decay width is model-dependent and may be chosen so that X decays outside the detector. The branching fraction $\mathcal{B}(B \rightarrow KX)$ is determined by the vector coupling bsX , while the axial-vector coupling determines its contribution to $B \rightarrow K^* X$. Flavor-violating axion couplings naturally occur in flavor models [14] and their phenomenology has been studied in detail in Ref. [15].

Higgs-like scalars [16–19] acquire the bsX coupling through their mixing with the SM Higgs boson, which also determines their decays to SM particles. This results in strong constraints from searches with displaced vertices, such as $B \rightarrow K^{(*)} X (\rightarrow \mu^+ \mu^-)$ [20–22]. These constraints can be avoided by introducing an additional decay channel to SM-singlet fermions [16], which suppresses $\mathcal{B}(X \rightarrow \mu^+ \mu^-)$. In multi-Higgs models, the scalar X can mix with different Higgs bosons, which removes the tight relationship between the couplings of X and avoids constraints from visible decays [7, 23–25].

The proposed models with vector bosons include τ -philic gauge bosons [2, 26] and dark gauge bosons [11, 27]. τ -philic gauge bosons predominantly decay invisibly into τ neutrinos and escape the Belle II detector. Dark gauge bosons acquire a bsX coupling by mixing with the Z boson. Avoiding constraints from visible decays into

* lorenz.gaertner@lmu.de

† nikolai.hartmann@physik.uni-muenchen.de

‡ thomas.kuhr@lmu.de

§ m.schmidt@unsw.edu.au

¶ slavomira.stefkova@uni-bonn.de

** bruce.yabsley@sydney.edu.au

SM fermions requires a large invisible decay width into dark sector particles. A detailed discussion of the flavor phenomenology of light dark vector bosons is provided in Ref. [28].

All discussed models have a small bsX coupling; for example, the dimensionless bsX gauge coupling of the $B_3 - L_3$ gauge boson is $\mathcal{O}(10^{-8})$ [2] and the effective decay constant in the axion-like particle scenario is $\mathcal{O}(10^8 \text{ GeV})$ [2, 11]. Similarly, existing models have only considered a small decay width with $\Gamma_X \ll m_X$. For a strongly coupled dark sector boson, the decay width Γ_X could be comparable to the mass, $\Gamma_X \sim m_X$.

To illustrate this point, consider two scenarios: a Higgs-like scalar and a dark gauge boson mixing with the Z boson, where the X invisible width is constrained by invisible Higgs and Z boson decays, respectively. The invisible decay width of a Higgs-like scalar is constrained to $\Gamma_X^{\text{inv}} \lesssim 0.2 m_X (4 \times 10^{-3} / \sin \theta)^2 (\mathcal{B}(h \rightarrow \text{inv}) / 0.107)$ [16] in terms of the scalar mixing angle θ and the invisible branching ratio of the SM Higgs, $\mathcal{B}(h \rightarrow \text{inv}) \leq 0.107$ at 95% C.L. [29]. Similarly, the invisible width of a dark gauge boson X mixing with the Z boson is given by $\Gamma_X^{\text{inv}} \simeq \alpha_X m_X / 6 \lesssim N_\nu \Gamma(Z \rightarrow \nu \bar{\nu}) m_X / 4 m_Z \epsilon_Z^2$ [11, 30], where α_X is the dark fine structure constant and $N_\nu = 2.9963 \pm 0.0074$ [31, 32] is the number of neutrinos. Due to the small $X - Z$ mixing angle $\epsilon_Z \simeq 10^{-4.6}$ [11] required to explain the excess, the constraint from the number of neutrinos N_ν is weaker than the requirement of a perturbative dark gauge coupling.

In conclusion, the X invisible width Γ_X^{inv} can be as large as 0.4 GeV for a Higgs-like scalar and even comparable to the mass for a dark gauge boson mixing with the Z boson. Consequently, the analysis considers both narrow and broad decay widths. Note that the large decay width has to arise predominantly from decays to particles escaping the detector, and hence is an invisible decay width.

III. ANALYSIS AND REINTERPRETATION METHOD

A. Belle II $B^+ \rightarrow K^+ \nu \bar{\nu}$ analysis

The Belle II $B^+ \rightarrow K^+ \nu \bar{\nu}$ analysis [1] uses two complementary strategies on nearly orthogonal datasets from $e^+ e^- \rightarrow \Upsilon(4S) \rightarrow B^+ B^-$: an inclusive tagging analysis (ITA) and a hadronic tagging analysis (HTA). The ITA reconstructs the K^+ and infers missing energy using two boosted decision trees (BDT₁, BDT₂) for background suppression, achieving high efficiency. The HTA fully reconstructs the companion B and applies one classifier (BDTh), yielding lower background at the price of a reduced efficiency.

The $B^+ \rightarrow K^+ \nu \bar{\nu}$ signal is based on a SM kinematic prediction [33], scaled by a normalization factor μ_{SM} . A *HistFactory* [34] likelihood implemented in

pyhf [35, 36] uses 4×3 bins in $\eta(\text{BDT}_2) \times q_{\text{rec}}^2$ (ITA)¹ and 6 bins in $\eta(\text{BDTh})$ (HTA), with an off-resonance control region (ITA) constraining continuum backgrounds. The combined fit with 231 nuisance parameters yielded $\mu_{\text{SM}} = 4.6 \pm 1.3$, corresponding to $\mathcal{B}(B^+ \rightarrow K^+ \nu \bar{\nu}) = (2.3 \pm 0.5(\text{stat})_{-0.4}^{+0.5}(\text{syst})) \cdot 10^{-5}$, with 3.5σ significance over background-only and 2.7σ over the SM (based on HPQCD form factors [37]).

B. Model-agnostic likelihood

The measurement is reinterpreted using a model-agnostic likelihood that isolates reconstruction effects from kinematic variations [8, 38]. The key ingredient is the joint number density $\nu_0(x, z)$, which represents the expected event distribution in reconstructed bins x for a kinematic variable z under a null hypothesis $\sigma_0(z)$. This density encodes everything from detector response to analysis procedure, effectively folding theoretical distributions into reconstructed ones.

For an alternative theory with kinematic prediction $\sigma_1(z)$, expected rates are obtained by reweighting: $\nu_1(x) = \int dz \nu_0(x, z) w(z)$, with $w(z) = \sigma_1(z) / \sigma_0(z)$. A discrete sum is used, $\nu_{1,x} = \sum_z \nu_{0,xz} w_z$, which is computationally fast and requires only the precomputed joint density and the ratio of predictions.

The variable $z = q^2$ represents the true dineutrino invariant mass squared, and x corresponds to the analysis bins: $\eta(\text{BDT}_2) \times q_{\text{rec}}^2$ (ITA) and $\eta(\text{BDTh})$ (HTA). The joint density uses 100 q^2 bins (plus one negative- q^2 bin for events outside this range due to issues with Monte Carlo truth matching) derived from SM signal simulation. The reweighting is implemented as a custom modifier in the pyhf/*HistFactory* framework, combined with the published $B^+ \rightarrow K^+ \nu \bar{\nu}$ likelihood.

The method's main limitation arises when $\sigma_1(z)$ is substantially larger than $\sigma_0(z)$, inflating weights and reducing effective precision. Here this effect is minimal with weights $w(z) < 5$.

C. Signal model

To test a light invisible resonance contributing to the $B^+ \rightarrow K^+ \nu \bar{\nu}$ signal, the decay $B^+ \rightarrow K^+ X$ with X invisible is modeled. A two-body resonance produces a peak at $q^2 = m_X^2$, described by a relativistic Breit-

¹ The reconstructed q^2 is defined as $q_{\text{rec}}^2 = \frac{s}{4} + M_K^2 - \sqrt{s} E_K^*$, where \sqrt{s} is the center-of-mass collision energy, M_K is the nominal kaon mass and E_K^* is the reconstructed energy of the kaon in the collision center-of-mass frame. The signal B meson is assumed to be at rest in the $e^+ e^-$ center-of-mass frame.

Wigner density:

$$f_{BW}(q^2|m_X, \Gamma_X) = \frac{k}{(q^2 - m_X^2)^2 + m_X^2 \Gamma_X^2}, \quad (1)$$

$$k = \frac{m_X \Gamma_X}{\pi/2 + \arctan(m_X/\Gamma_X)},$$

where m_X is the resonance mass, Γ_X is the decay width and k ensures normalization. Since both the B and K mesons are spinless, the decay kinematics do not depend on the spin of the boson X . Consequently, the analysis is insensitive to this quantity.

Adding the two-body model to the $B^+ \rightarrow K^+ \nu \bar{\nu}$ SM expectation,

$$\sigma_0(q^2) = \mu_{SM} \frac{d\mathcal{B}_{SM}}{dq^2}, \quad (2)$$

the total differential branching fraction is

$$\sigma_1(q^2) = \frac{d\mathcal{B}}{dq^2} = \mu_{SM} \frac{d\mathcal{B}_{SM}}{dq^2} + \mu_X \rho_X f_{BW}(q^2|m_X, \Gamma_X), \quad (3)$$

with SM signal strength μ_{SM} , new-physics signal strength μ_X , and $\rho_X = 10^{-6}$ for numerical stability, such that $\mathcal{B}(B^+ \rightarrow K^+ X) \mathcal{P}_{X,\text{inv}} = \mu_X \rho_X$, where $\mathcal{P}_{X,\text{inv}} = \mathcal{P}_{X,\text{out}} + (1 - \mathcal{P}_{X,\text{out}}) \cdot \mathcal{B}(X \rightarrow \text{inv})$ is the sum of the probability for the particle to decay outside the detector coverage, $\mathcal{P}_{X,\text{out}}$, and the probability to decay invisibly inside the detector coverage (see, e.g., Ref. [39]). For the large invisible X decay widths considered in this analysis, $\mathcal{P}_{X,\text{inv}} \approx \mathcal{B}(X \rightarrow \text{inv})$.

The $B^+ \rightarrow K^+ \nu \bar{\nu}$ SM contribution is treated as background. The parameter μ_{SM} is constrained around unity with a 5% normalization uncertainty (added to other systematics), accounting for a 4.4% uncertainty on the product of CKM matrix elements $|V_{ts}^* V_{tb}|^2$ and a 2.3% uncertainty on the contributing Wilson coefficient $|C_{V\bar{L}}^{\text{SM}}|^2$ [33]. The SM input uses the HPQCD form factors [37].

The parameters μ_X and m_X are inferred for two fixed widths, $\Gamma_X \in \{0.1, 0.5\}$ GeV. The coarse q_{rec}^2 binning used in the Belle II analysis [1] limits the sensitivity to narrow structures in the spectrum. As a result, widths below ~ 0.1 GeV produce bin-averaged distributions that are indistinguishable from the case $\Gamma_X = 0.1$ GeV. This value effectively represents the narrow-width limit and covers all narrow-width models discussed above. The broader width $\Gamma_X = 0.5$ GeV tests a strongly coupled boson which can be realized in scenarios such as Higgs-like scalars or dark gauge bosons. A future Belle II analysis with finer q_{rec}^2 binning would significantly improve the mass resolution. Figure 1 shows the predicted differential branching fraction for both widths, assuming $\mu_X = 1$, $m_X = 2$ GeV.

IV. POSTERIOR AND CREDIBLE INTERVALS

This section presents the Bayesian reinterpretation of the Belle II $B^+ \rightarrow K^+ \nu \bar{\nu}$ measurement using the signal model described in Eq. (3). Posterior distributions

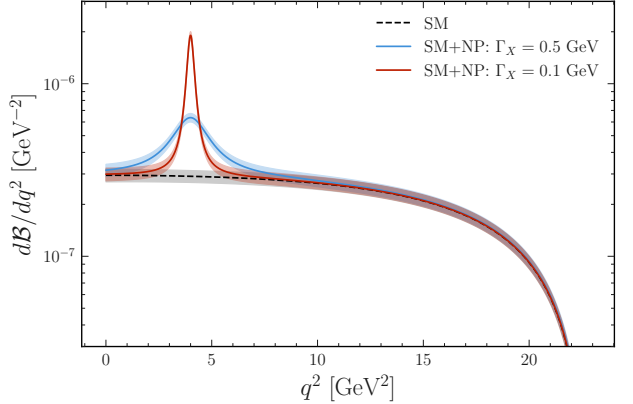


Figure 1. Predicted differential branching fraction from Eq. (3) for two resonance widths at $\mu_X = 1$, $m_X = 2$ GeV. Bands include hadronic form-factor and 5% SM normalization uncertainties. Form factor uncertainties on the resonance contribution are not considered.

and credible intervals are derived for the signal strength μ_X and mass m_X , assuming fixed resonance widths of $\Gamma_X = 0.1$ and 0.5 GeV.

The `HistFactory` likelihood [34] is translated into a Bayesian posterior for inference,

$$f(\boldsymbol{\eta}, \boldsymbol{\chi} | \mathbf{n}, \mathbf{a}) \propto f(\mathbf{n} | \boldsymbol{\nu}(\boldsymbol{\eta}, \boldsymbol{\chi})) f(\boldsymbol{\chi} | \mathbf{a}) f(\boldsymbol{\eta}). \quad (4)$$

Here, $f(\mathbf{n} | \boldsymbol{\nu}(\boldsymbol{\eta}, \boldsymbol{\chi}))$ is the likelihood, given observed and expected bin yields \mathbf{n} and $\boldsymbol{\nu}(\boldsymbol{\eta}, \boldsymbol{\chi})$, respectively; $f(\boldsymbol{\chi} | \mathbf{a})$ encodes priors for nuisance parameters $\boldsymbol{\chi}$ using auxiliary data \mathbf{a} (normally distributed), and $f(\boldsymbol{\eta})$ specifies priors for unconstrained parameters $\boldsymbol{\eta}$. Prior distributions for the parameters of interest are chosen to be uniform over the ranges specified in Table I. Ranges are chosen to cover the full posterior, as verified a posteriori. Appendix A examines the robustness of the results with respect to alternative prior choices. The posterior is implemented and sampled with `bayesian pyhf` [40] using `pymc` [41] as the back end.

Table I. Prior ranges for the new-physics signal strength μ_X and resonance mass m_X , for the two resonance widths.

$\Gamma_X =$	0.1 GeV	0.5 GeV
μ_X	[0.0, 24.0]	[0.0, 32.0]
m_X [GeV]	[1.5, 3.0]	[1.5, 3.2]

Marginal posteriors for μ_X and m_X are obtained by sampling the joint posterior with Markov Chain Monte Carlo and marginalizing over nuisance parameters. Figure 2 shows 1- and 2-dimensional marginal distributions for the two widths, with contours enclosing 68% and 95% credible regions.

From 1-dimensional marginal distributions, highest density intervals (HDIs) are calculated at 68% and 95%

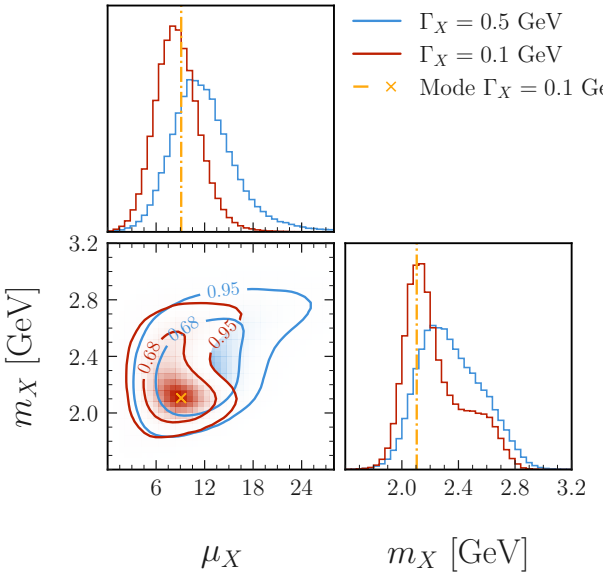


Figure 2. Marginalized posterior distributions for $B^+ \rightarrow K^+ X$ model parameters from Eq. (3) for two resonance widths $\Gamma_X = 0.1$ and 0.5 GeV. Diagonal panels show 1-dimensional densities; the off-diagonal panel shows 2-dimensional densities (linear scale). Contours enclose 68% and 95% credible regions. The dash-dotted yellow lines and cross mark the posterior mode.

probability. Table II summarizes posterior modes and credible intervals.

Table II. Posterior mode and HDIs at 68% and 95% credible levels for $B^+ \rightarrow K^+ X$ model parameters from Eq. (3), derived from Fig. 2. The product of branching fractions is $\mathcal{B}(B^+ \rightarrow K^+ X) \cdot \mathcal{P}_{X,\text{inv}} = \mu_X \cdot 10^{-6}$.

Param.	Γ_X [GeV]	Mode	68% HDI	95% HDI
μ_X	0.1	9.2	[5.8, 11.0]	[3.4, 14.0]
	0.5	11.1	[7.8, 15.0]	[4.2, 20.2]
m_X [GeV]	0.1	2.1	[2.0, 2.3]	[1.9, 2.7]
	0.5	2.2	[2.1, 2.5]	[2.0, 2.8]

Direct comparison of the observed data with the predicted yields at the posterior mode for the unconstrained $B^+ \rightarrow K^+ \nu \bar{\nu}$ SM (μ_{SM} unconstrained, $\mu_X = 0$) and $B^+ \rightarrow K^+ X$ ($\Gamma_X = 0.1$ GeV) models is illustrated in Fig. 3, for the highest sensitivity region of the analysis (ITA, $\eta(\text{BDT}_2) > 0.98$). The $B^+ \rightarrow K^+ X$ model fits the data significantly better than the unconstrained SM prediction, as indicated by the smaller pull values.

For the considered widths, m_X peaks sharply at $2.1 - 2.2$ GeV with an extended tail toward higher masses. The peak location is consistent across widths, indicating the data favor a resonance in this range regardless of the assumed width. This agrees with the excess observed in

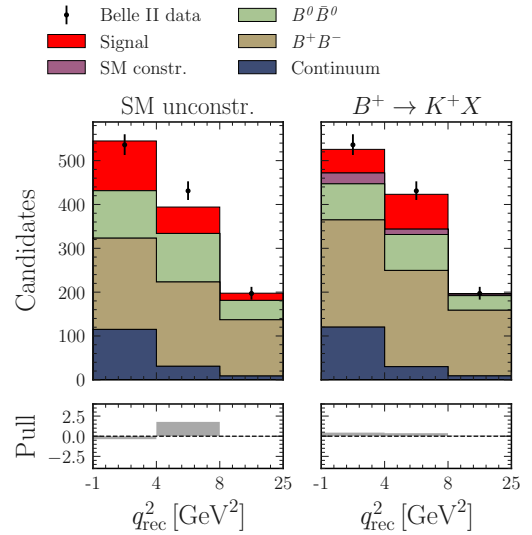


Figure 3. Observed and predicted best-fit yields in the highest sensitivity region. Signal predictions are for the unconstrained $B^+ \rightarrow K^+ \nu \bar{\nu}$ SM (left) and $B^+ \rightarrow K^+ X$ with $\Gamma_X = 0.1$ GeV (right). For $B^+ \rightarrow K^+ X$, the constrained $B^+ \rightarrow K^+ \nu \bar{\nu}$ SM background is shown separately. Background yields include neutral and charged B -meson decays and summed continuum categories. Lower panels show pulls.

Ref. [1] and its interpretations presented in Refs. [2, 3, 5].

The new-physics signal strength μ_X deviates clearly from zero for both widths, indicating a preference for a non-zero $B^+ \rightarrow K^+ X$ contribution. Posterior modes increase with width: $\mu_X = 9.2$ and 11.1 for $\Gamma_X = 0.1$ and 0.5 GeV, respectively. This is expected because broader resonances distribute the same total rate over a larger q^2 range, requiring higher normalization to match the observed excess.

The narrow resonance ($\Gamma_X = 0.1$ GeV) yields

$$\mathcal{B}(B^+ \rightarrow K^+ X) \cdot \mathcal{P}_{X,\text{inv}} = 9.2^{+1.8}_{-3.4} \cdot 10^{-6}, \quad (5)$$

roughly twice the $B^+ \rightarrow K^+ \nu \bar{\nu}$ SM expectation $\mathcal{B}_{\text{SM}} = (4.97 \pm 0.37) \cdot 10^{-6}$ [33].

V. UPPER LIMIT MASS SCAN

A modified frequentist scan over the resonance mass m_X is performed to derive 95% confidence level upper limits on the product of branching fractions $\mathcal{B}(B^+ \rightarrow K^+ X) \cdot \mathcal{P}_{X,\text{inv}}$. The confidence limit is determined using the CL_s criterion [42],

$$CL_s = \frac{p(q_{\text{obs}} \mid B^+ \rightarrow K^+ X + \text{SM})}{p(q_{\text{obs}} \mid \text{SM})} = 0.05. \quad (6)$$

Here q_{obs} is the upper limit test statistic evaluated on data, and $p(q_{\text{obs}} \mid B^+ \rightarrow K^+ X + \text{SM})$ and $p(q_{\text{obs}} \mid \text{SM})$ are the corresponding p -values under the $B^+ \rightarrow K^+ X + \text{SM}$ and SM-only hypotheses, respectively.

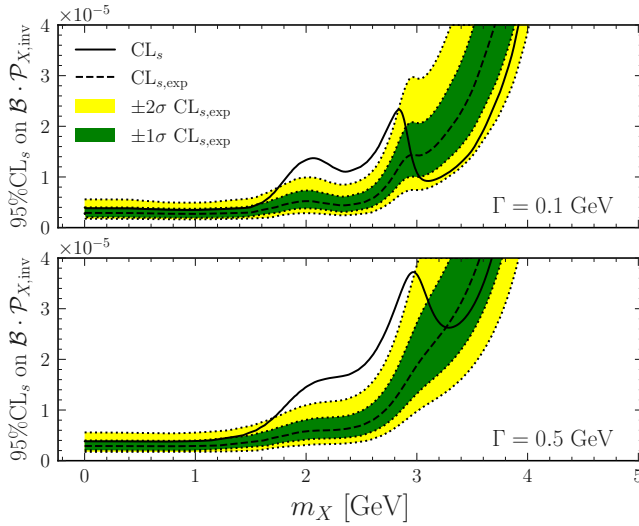


Figure 4. Modified frequentist 95% CL_s upper limit on $\mathcal{B}(B^+ \rightarrow K^+ X) \cdot \mathcal{P}_{X,inv}$ as a function of m_X (solid black), compared to the expected SM limit (dashed black) with $\pm 1\sigma$ (green) and $\pm 2\sigma$ (yellow) bands.

Figure 4 shows the observed and expected limits. The observed limit exceeds the SM expectation by over 2 standard deviations in the mass range $m_X \in [1.8, 2.8]$ GeV for $\Gamma_X = 0.1$ GeV, and $m_X \in [1.7, 3.0]$ GeV for $\Gamma_X = 0.5$ GeV.

These numerical results agree well with the upper credible intervals from Section IV. The observed upper limits exhibit a similar shape as the contours of the 2-dimensional posterior in Fig. 2.

At higher masses ($m_X > 3.5$ GeV), sensitivity degrades due to reduced experimental efficiency. Localized features in the expected limit near 2 and 3 GeV correspond to analysis bin boundaries.

These results are compared to the preliminary dedicated search for $B \rightarrow KX$ using 711 fb^{-1} Belle data [43]. This reinterpretation yields stronger constraints in the low-mass region and uniquely retains sensitivity around $m_X \approx 2$ GeV, a region excluded in the dedicated search. Conversely, the dedicated analysis achieves superior sensitivity at high masses.

VI. GOODNESS-OF-FIT

The fit quality of the $B^+ \rightarrow K^+ X$ hypothesis is assessed with a saturated-likelihood statistic:

$$p_{\text{gof}} = \int_{t_{\text{obs}}}^{\infty} dt_{\text{gof}} f(t_{\text{gof}}), \quad t_{\text{gof}} = -2 \ln \frac{f(\mathbf{n}, \mathbf{a} | \hat{\boldsymbol{\eta}}, \hat{\boldsymbol{\chi}})}{f_{\text{sat}}(\mathbf{n}, \mathbf{a} | \bar{\boldsymbol{\chi}})}, \quad (7)$$

where $f(\mathbf{n}, \mathbf{a} | \hat{\boldsymbol{\eta}}, \hat{\boldsymbol{\chi}})$ is the likelihood at the global best fit, and f_{sat} is the saturated likelihood that represents a perfect fit to the observed data.

The sampling distribution $f(t_{\text{gof}})$ is obtained from fits

to toy data generated at the best fit of each $B^+ \rightarrow K^+ X$ width [44], and p_{gof} is the fraction with $t > t_{\text{obs}}$.

The goodness-of-fit values, summarized in Table III, are high and nearly width-independent: $p_{\text{gof}} = 0.83, 0.82$ for $\Gamma_X = 0.1$ and 0.5 GeV, respectively. Thus about 80% of toys yield worse fits than the data, indicating excellent fit quality. The weak dependence on Γ_X reflects the limited resolution due to the coarse q_{rec}^2 binning.

For comparison, the unconstrained SM yields $p_{\text{gof}} = 0.58$, which also indicates a good fit to the data.

Table III. Bayes factors relative to the background-only model (BKG) and the constrained SM, and goodness-of-fit p -values for $B^+ \rightarrow K^+ X$ at the two considered widths.

Model	Γ_X	$\log_{10} B_{\text{BKG}}$	$\log_{10} B_{\text{SM}}$	p_{gof}
$B^+ \rightarrow K^+ X$	0.1 GeV	2.82	1.71	0.83
$B^+ \rightarrow K^+ X$	0.5 GeV	2.93	1.83	0.82
unconst. SM	—	2.02	0.92	0.58

VII. MODEL COMPARISON

Model comparison quantifies the *relative* support for competing hypotheses. The $B^+ \rightarrow K^+ X$ model is assessed against two references: background-only ($\mu_{\text{SM}} = \mu_X = 0$) and the constrained SM (μ_{SM} constrained, $\mu_X = 0$), using Bayes factors and frequentist hypothesis testing.

Bayesian comparison uses the Bayes factor (ratio of marginal likelihoods) [45]. For $\Gamma_X = 0.1$ and 0.5 GeV the values are $\log_{10} B_{\text{SM}} = 1.71$ and 1.83 (*very strong* preference over the constrained SM on Jeffreys' scale [46]) and $\log_{10} B_{\text{BKG}} = 2.82$ and 2.93 (*decisive* preference over the background-only hypothesis). The $B^+ \rightarrow K^+ X$ model is preferred over the unconstrained SM (see Table III), consistent with a resonance better capturing the excess near $q_{\text{rec}}^2 \sim 3\text{--}7$ GeV². Because the marginal likelihood integrates over the full parameter space, these Bayes factors already include the look-elsewhere effect [47] and thus represent global, not merely local, preference for $B^+ \rightarrow K^+ X$.

To complement the Bayesian comparison, $B^+ \rightarrow K^+ X$ is tested against the constrained SM with a likelihood-ratio statistic and toy-based p -values:

$$p = \int_{t_{\text{obs}}}^{\infty} dt f(t), \quad t = -2 \ln \frac{f(\mathbf{n}, \mathbf{a} | \boldsymbol{\eta} = \mathbf{0}, \hat{\boldsymbol{\chi}})}{f(\mathbf{n}, \mathbf{a} | \hat{\boldsymbol{\eta}}, \hat{\boldsymbol{\chi}})}, \quad (8)$$

where $f(\mathbf{n}, \mathbf{a} | \hat{\boldsymbol{\eta}}, \hat{\boldsymbol{\chi}})$ is the global best fit and $f(\mathbf{n}, \mathbf{a} | \boldsymbol{\eta} = \mathbf{0}, \hat{\boldsymbol{\chi}})$ fixes the parameters of interest to their null values while optimizing nuisances. The sampling distribution $f(t)$ is obtained from toys generated under the SM hypothesis, and p is the fraction with $t > t_{\text{obs}}$.

For $B^+ \rightarrow K^+ X$ with $\Gamma_X = 0.1$ GeV, the resulting p -value is $1.4 \cdot 10^{-3}$ —a 3.0σ deviation from the SM. This exceeds the 2.7σ in Ref. [1] because the $B^+ \rightarrow K^+ X$ shape

matches the observed excess better than an overall enhancement of the SM distribution.

The look-elsewhere effect is included, as toys are drawn under the constrained $B^+ \rightarrow K^+ \nu \bar{\nu}$ SM and each fit floats μ_X and m_X .

VIII. CONCLUSION

This work presents a reinterpretation of the Belle II measurement of $B^+ \rightarrow K^+ \nu \bar{\nu}$ using the published model-agnostic likelihood to test the hypothesis of a two-body decay $B^+ \rightarrow K^+ X$ into a light invisible boson X . The data strongly prefer the resonance hypothesis, with a posterior mode for the mass at $m_X = 2.1^{+0.2}_{-0.1}$ GeV and a branching fraction $\mathcal{B}(B^+ \rightarrow K^+ X) \cdot \mathcal{P}_{X,\text{inv}} = 9.2^{+1.8}_{-3.4} \cdot 10^{-6}$. A modified frequentist mass scan confirms the excess is localized around $m_X \approx 2.1$ GeV, consistent with the Bayesian results, and provides the most stringent upper limits for the $m_X < 2.1$ GeV region to date.

Bayesian model comparison indicates a very strong preference for the $B^+ \rightarrow K^+ X$ model over the constrained SM and a decisive preference over the background-only hypothesis. A complementary frequentist hypothesis test favors $B^+ \rightarrow K^+ X$ over the constrained SM at 3.0σ . This significance exceeds the 2.7σ reported by the Belle II collaboration [1] because the kinematic shape of the resonance better matches the observed excess than the unconstrained SM.

The central values for the mass and branching fraction are consistent with previous reinterpretations based on simplified likelihoods [2, 3, 5]. While uncertainty intervals vary across studies, this analysis uniquely incorporates full experimental uncertainties, providing the most robust estimates to date.

The analysis demonstrates that a light invisible resonance provides an excellent description of the Belle II data, significantly outperforming the SM. This motivates further measurements to clarify the presence of contributions beyond the SM.

IX. ACKNOWLEDGMENTS

The authors thank Danny van Dyk and Méril Reboud for their contributions during the initial stages of this project. We thank Emmanuel Stamou for reviewing the manuscript.

Gärtner is funded by the Deutsche Forschungsgemeinschaft (DFG, German Research Foundation) – project number 460248186 (PUNCH4NFDI). Krug is supported by the Excellence Cluster ORIGINS, which is funded by the Deutsche Forschungsgemeinschaft (DFG, German Research Foundation) under Germany’s Excellence

Strategy - EXC-2094-39078331. Kuhr acknowledges the support of the German Federal Ministry of Research, Technology and Space (BMFTR). Stefkova acknowledges the support of the German Federal Ministry of Research, Technology and Space (BMFTR) and Excellence Cluster Color Meets Flavor, which is funded by the Deutsche Forschungsgemeinschaft (DFG, German Research Foundation) under Germany’s Excellence Strategy - EXC-3107-533766364. Yabsley acknowledges the support of The University of Sydney Physics Foundation.

Appendix A: Prior sensitivity study

Bayesian inference depends on prior distributions. Robustness is assessed by comparing baseline uniform priors to two alternative specifications for the $B^+ \rightarrow K^+ X$ model (Eq. (3)) with $\Gamma_X = 0.1$ GeV.

The first alternative uses a *truncated-normal prior* for μ_X and a uniform prior for m_X :

$$f(\mu_X) = \begin{cases} \mathcal{N}(\mu_X | \mu = 0, \sigma = 20) & \mu_X \geq 0 \\ 0 & \mu_X < 0 \end{cases}, \quad (A1)$$

$$f(m_X) = \mathcal{U}([1.5, 3.0] \text{ GeV}),$$

where \mathcal{U} denotes a uniform distribution.

The second alternative adopts a *uniform prior in squared mass m_X^2* , yielding a triangular prior in m_X :

$$f(\mu_X) = \mathcal{U}([0, 24]),$$

$$f(m_X) \propto \begin{cases} m_X & m_X \leq 4.8 \text{ GeV} \\ 0 & m_X > 4.8 \text{ GeV.} \end{cases} \quad (A2)$$

Table IV summarizes posterior modes and credible intervals for both alternatives. The mass m_X is robustly determined: the posterior mode ($m_X = 2.1$ GeV) and credible intervals show minimal prior sensitivity. The new-physics signal strength μ_X shifts slightly from 9.2 (uniform) to 9.0 (truncated-normal and triangular), with similarly robust credible intervals.

Table IV. Posterior modes, and 68%/95% HDIs for $B^+ \rightarrow K^+ X$ model (Eq. (3)) with $\Gamma_X = 0.1$ GeV based on alternative priors (compare Table II).

Priors	Param.	Mode	68% HDI	95% HDI
Eq. (A1)	μ_X	9.0	[5.7, 10.8]	[3.4, 13.8]
	m_X [GeV]	2.1	[2.0, 2.4]	[1.9, 2.7]
Eq. (A2)	μ_X	9.0	[5.7, 11.0]	[3.0, 14.4]
	m_X [GeV]	2.1	[2.0, 2.4]	[1.9, 2.7]

[1] I. Adachi *et al.* (Belle II Collaboration), Phys. Rev. D **109**, 112006 (2024).

[2] W. Altmannshofer, A. Crivellin, H. Haigh, G. Inguglia, and J. M. Camalich, Phys. Rev. D **109**, 075008 (2024).

[3] K. Fridell, M. Ghosh, T. Okui, and K. Tobioka, Phys. Rev. D **109**, 115006 (2024), arXiv:2312.12507 [hep-ph].

[4] P. D. Bolton, S. Fajfer, J. F. Kamenik, and M. Novoa-Brunet, Phys. Rev. D **110**, 055001 (2024), [Erratum: Phys. Rev. D **111**, 039903 (2025)], arXiv:2403.13887 [hep-ph].

[5] P. D. Bolton, S. Fajfer, J. F. Kamenik, and M. Novoa-Brunet, Phys. Rev. D **112**, 035010 (2025), arXiv:2503.19025 [hep-ph].

[6] A. Berezhnoy, W. Lucha, and D. Melikhov, Phys. Rev. D **111**, 075035 (2025), arXiv:2502.14313 [hep-ph].

[7] A. Berezhnoy, W. Lucha, and D. Melikhov, (2025), arXiv:2507.10801 [hep-ph].

[8] M. Abumusab *et al.* (Belle II Collaboration), Phys. Rev. D **112**, 092016 (2025), arXiv:2507.12393 [hep-ex].

[9] Belle II Collaboration, A model-agnostic likelihood for the reinterpretation of the $B^+ \rightarrow K^+ \nu \bar{\nu}$ measurement at Belle II, HEPData (collection) (2025), <https://doi.org/10.17182/hepdata.166082>.

[10] W. Altmannshofer and S. Roy, Phys. Rev. D **111**, 075029 (2025), arXiv:2411.06592 [hep-ph].

[11] L. Calibbi, T. Li, L. Mukherjee, and M. A. Schmidt, Phys. Rev. D **112**, 075020 (2025), arXiv:2502.04900 [hep-ph].

[12] Q.-Y. Hu, Eur. Phys. J. C **85**, 556 (2025), arXiv:2412.19084 [hep-ph].

[13] X. Gao and U. Nierste, Phys. Rev. D **112**, 055008 (2025), arXiv:2506.14876 [hep-ph].

[14] F. Wilczek, Phys. Rev. Lett. **49**, 1549 (1982).

[15] J. Martin Camalich, M. Pospelov, P. N. H. Vuong, R. Ziegler, and J. Zupan, Phys. Rev. D **102**, 015023 (2020), arXiv:2002.04623 [hep-ph].

[16] M. Ovchynnikov, M. A. Schmidt, and T. Schwetz, Eur. Phys. J. C **83**, 791 (2023), arXiv:2306.09508 [hep-ph].

[17] D. McKeen, J. N. Ng, and D. Tuckler, Phys. Rev. D **109**, 075006 (2024), arXiv:2312.00982 [hep-ph].

[18] S.-Y. Ho, J. Kim, and P. Ko, Phys. Rev. D **111**, 055029 (2025), arXiv:2401.10112 [hep-ph].

[19] J. Kim and P. Ko, (2025), arXiv:2511.20430 [hep-ph].

[20] R. Aaij *et al.* (LHCb Collaboration), Phys. Rev. Lett. **115**, 161802 (2015), arXiv:1508.04094 [hep-ex].

[21] R. Aaij *et al.* (LHCb Collaboration), Phys. Rev. D **95**, 071101 (2017), arXiv:1612.07818 [hep-ex].

[22] I. Adachi *et al.* (Belle II Collaboration), Phys. Rev. D **108**, L111104 (2023), arXiv:2306.02830 [hep-ex].

[23] M. Abdughani and Y. Reyimuaji, Phys. Rev. D **110**, 055013 (2024), arXiv:2309.03706 [hep-ph].

[24] A. Berezhnoy and D. Melikhov, Europhys. Lett. **145**, 14001 (2024), arXiv:2309.17191 [hep-ph].

[25] A. Datta, D. Marfatia, and L. Mukherjee, Phys. Rev. D **109**, L031701 (2024), arXiv:2310.15136 [hep-ph].

[26] L. Di Luzio, M. Nardecchia, and C. Toni, Phys. Rev. D **112**, 055031 (2025), arXiv:2505.11499 [hep-ph].

[27] P. D. Bolton, J. F. Kamenik, and M. Novoa-Brunet, (2025), arXiv:2512.16999 [hep-ph].

[28] J. F. Eguren, S. Klingel, E. Stamou, M. Tabet, and R. Ziegler, JHEP **08**, 111, arXiv:2405.00108 [hep-ph].

[29] G. Aad *et al.* (ATLAS Collaboration), Phys. Lett. B **842**, 137963 (2023), arXiv:2301.10731 [hep-ex].

[30] H. Davoudiasl, H.-S. Lee, and W. J. Marciano, Phys. Rev. D **85**, 115019 (2012), arXiv:1203.2947 [hep-ph].

[31] S. Schael *et al.* (ALEPH, DELPHI, L3, OPAL, SLD, LEP Electroweak Working Group, SLD Electroweak Group, SLD Heavy Flavour Group), Phys. Rept. **427**, 257 (2006), arXiv:hep-ex/0509008.

[32] P. Janot and S. Jadach, Phys. Lett. B **803**, 135319 (2020), arXiv:1912.02067 [hep-ph].

[33] W. G. Parrott, C. Bouchard, and C. T. H. Davies (HPQCD Collaboration), Phys. Rev. D **107**, 014511 (2023), [Erratum: Phys. Rev. D **107**, 119903 (2023)], arXiv:2207.13371 [hep-ph].

[34] K. Cranmer, G. Lewis, L. Moneta, A. Shibata, and W. Verkerke (ROOT), *HistFactory: A tool for creating statistical models for use with RooFit and RooStats*, Tech. Rep. (New York U., New York, 2012).

[35] L. Heinrich, M. Feickert, G. Stark, and K. Cranmer, J. Open Source Software **6**, 2823 (2021).

[36] L. Heinrich, M. Feickert, and G. Stark, pyhf: v0.7.6 (2024), see also the GitHub webpage.

[37] W. G. Parrott, C. Bouchard, and C. T. H. Davies (HPQCD Collaboration), Phys. Rev. D **107**, 014510 (2023), arXiv:2207.12468 [hep-lat].

[38] L. Gärtner, N. Hartmann, L. Heinrich, M. Horstmann, T. Kuhr, M. Reboud, S. Stefkova, and D. van Dyk, Eur. Phys. J. C **84**, 693 (2024), arXiv:2402.08417 [hep-ph].

[39] T. Ferber, A. Filimonova, R. Schäfer, and S. Westhoff, J. High Energy Phys. **04**, 131 (2023), arXiv:2201.06580 [hep-ph].

[40] M. Feickert, L. Heinrich, and M. Horstmann, EPJ Web Conf. **295**, 06004 (2024), arXiv:2309.17005 [stat.CO].

[41] O. Abril-Pla, V. Andreani, C. Carroll, L. Dong, C. J. Fonnebeck, M. Kochurov, R. Kumar, J. Lao, C. C. Luhmann, O. A. Martin, *et al.*, PeerJ Comput. Sci. **9** (2023).

[42] A. L. Read, J. Phys. G **28**, 2693 (2002).

[43] Belle and Belle II Collaborations (2025), presented at the 13th International Workshop on the CKM Unitarity Triangle (CKM 2025), Cagliari, Italy.

[44] K. Cranmer, in *2011 European School of High-Energy Physics* (2014) pp. 267–308, arXiv:1503.07622 [physics.data-an].

[45] A. Gelman, J. Carlin, H. Stern, D. Dunson, A. Vehtari, and D. Rubin, *Bayesian Data Analysis, Third Edition*, Chapman & Hall/CRC Texts in Statistical Science (Taylor & Francis, 2013).

[46] H. Jeffreys, *The Theory of Probability*, 3rd ed. (Oxford University Press, 1961).

[47] E. Gross and O. Vitells, Eur. Phys. J. C **70**, 525 (2010), arXiv:1005.1891 [physics.data-an].